Morphology and Properties of Isotactic Polypropylene Modified with Hydrocarbon Resin MBG273. I. Binary Blends

S. Cimmino, C. Silvestre, G. della Vecchia

Istituto di Chimica e Tecnologia dei Polimeri, Consiglio Nazionale delle Richerche (CNR), Via Campi Flegrei 34, 80074, Pozzuoli (NA), Italy

Received 9 April 2003; accepted 15 January 2004

ABSTRACT: We investigated a system formed of isotactic polypropylene (iPP) and hydrogenated hydrocarbon resin MBG273 (up to 30 wt % resin) to study the influence of the composition on the morphology, structure, and properties of its blends and derived films. All the blends, after the mixing of the components in the melt and cooling at room temperature, were formed by a crystalline phase of iPP and by one homogeneous phase formed by amorphous iPP and the MBG273 resin. The presence of MBG273 did not influence the crystalline structure of iPP, which remained, for every blend, α-monoclinic, but it reduced the crystallization temperature and nucleation density of iPP. Differential scanning calorimetry and dynamic mechanical thermal analysis showed an increase in the glass-transition temperature with the resin content, confirming the formation of one amorphous phase. Tensile property analysis indicated an increase in Young's modulus and a decrease in the elongation at break of films as a function of the resin content in the blends. The water vapor permeability and tensile mechanical properties were related to an increase in the glass transition with the addition of MBG273. © 2004 Wiley Periodicals, Inc. J Appl Polym Sci 92: 3454–3465, 2004

Key words: poly(propylene) (PP); resins; morphology; thermal properties; mechanical properties

INTRODUCTION

Isotactic polypropylene (iPP) is a polymer widely used for packaging because of the low cost of its film-production process, its good mechanical properties (high elastic modulus), its good optical properties (transparency and gloss), and its low permeability to gases and aromas. Despite this, exigent and pressing market demands require increased intrinsic film properties and technological processing properties. Research groups, in collaboration with industry, are studying polymer systems based on a matrix of iPP modified with natural resins, such as terpene resins[1–4] [poly(α-pinene) (PαP), poly(β-pinene) (PβP), and poly(*d*-limonene) (PL)], and synthetic resins,[5–13] such as hydrogenated oligocyclopentadiene (HOCP). In addition to their commercial importance, the new products have attracted scientific interest. The two components iPP and HOCP are partially miscible. In fact, a pseudophase diagram presenting both lower and upper cloud-point curves has been determined, and it shows that films with different phase structures, morphologies, and properties can be obtained.[8] Moreover, films with different properties can be obtained according to the parameters used for the preparation of the films, such as the blend composition, temperature of mixing, and cooling rate from the melt. Also, natural terpene resins are partially miscible with iPP.[1] In fact, PαP is miscible with iPP up to an 80/20 composition, whereas PL and PβP[4] are miscible with iPP up to a 90/10 composition. Blends with higher resin contents are partially miscible; that is, the amorphous phase is formed by two conjugated phases: (1) an iPP-rich phase and (2) a resin-rich phase. These studies have indicated that the addition to iPP of a resin (5–20 wt %) will generally induce the modification of the film properties, producing, for example, higher elastic modulus, improved optical properties (e.g., higher transparency and gloss), lower permeability to gases, water vapor, and aromas, and lower melt viscosity (this allows the mixing temperature to be reduced and thus reduces the energy consumption and polymer degradation). The use of these resins in polymers that come into contact with food for human consumption is regulated by the Food and Drug Administration of the U.S. Department of Health, Education, and Welfare.

This work continues the study of blends of iPP with resins for plastic modification, particularly dealing with the investigation of iPP modified with a petroleum hydrogenated hydrocarbon resin (HR), MBG273, from Eastman Chemical Co. (The Hague, The Netherlands).

Correspondence to: S. Cimmino (cimmino@irtemp.na.cnr.it).

Journal of Applied Polymer Science, Vol. 92, 3454–3465 (2004)
© 2004 Wiley Periodicals, Inc.

Petroleum HRs[14] comprise a class of synthetic polymer products derived from a variable mixture of unsaturated monomers obtained as volatile byproducts in the cracking of natural gas, gas oil, or petroleum naphtha. The unsaturated monomers consist of monoolefins and diolefins (pentenes, hexenes, heptenes, pentadiene, and hexadienes), cyclic olefins and diolefins (cyclopentene, cyclopentadiene, methylcyclopentadiene, cyclohexene, and cyclohexadiene) and vinyl derivatives of aromatic hydrocarbons (styrene, α-methylstyrene, vinyl toluenes, indene, and methyl indenes).

All petroleum HRs have the following properties in common: water resistance, wide compatibility with other resins, solubility in low-cost solvents, chemical neutrality, good electrical properties, and nonsaponifiability. Commercial HRs are commonly characterized by their color, softening point, iodine number, specific gravity, solution viscosity, and aniline point.

A hydrogenated HR is an oligomer obtained in three steps: the polymerization of monomers such as styrene, α-methylstyrene, vinyl toluene, cyclopentadiene, and indene to form an aromatic precursor resin; a weak hydrogenation reaction to saturate the backbone along the chain; and a strong hydrogenation reaction to destroy the aromaticity of the ring to create a fully alicyclic resin.

The aim of this research was to investigate the influence of the hydrogenated HR MBG273 on the morphology and structure of iPP/HR blends and derived films as a function of the blend composition and to correlate them with the thermal, mechanical, and water vapor permeability properties.

EXPERIMENTAL

Materials

The materials used were (1) commercial iPP (Moplen X30S), produced by Montell (Basell, Ferrara, Italy) (weight-average molecular weight = 3.5×10^5 g/mol, number-average molecular weight = 4.69×10^4 g/mol, z-average molecular weight = 2.06×10^6 g/mol, melt-flow index = 9 g/10 min, density = 0.9 g/cm^3), and (2) the hydrogenated HR MBG273, produced and kindly supplied by Eastman Chemical Co. (weight-average molecular weight = 1.47×10^3 g/mol, number-average molecular weight = 9.0×10^2 g/mol, z-average molecular weight = 2.4×10^3 g/mol) in the following formula:

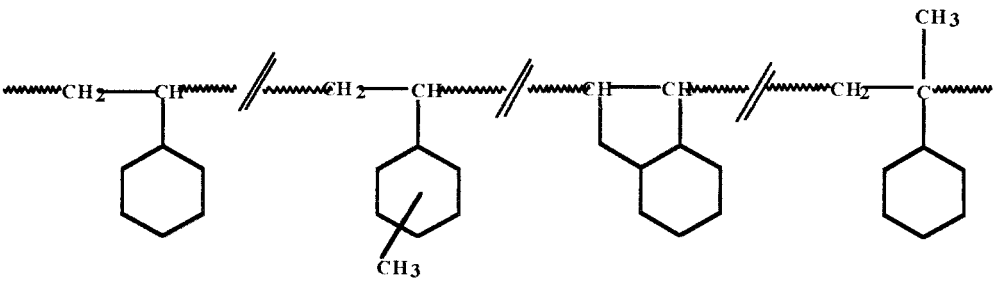

The glass-transition temperature (T_g) of the HR MBG273 resin was detected at about 82°C by differential scanning calorimetry (DSC).

Blend preparation

HR MBG273 and iPP were mixed in a Rheocord EC Brabender-like apparatus (Haake, Inc., Saddle Brook, NJ) at 210°C and 32 rpm for 10 min. The compositions of the iPP/HR blends were 100/0, 97.5/2.5, 95/5, 90/10, 85/15, 80/20, and 70/30 w/w.

Preparation of the compression-molded samples

Films 65–75 μm thick, used for dynamic mechanical thermal analysis (DMTA) and water vapor permeability testing, were prepared by compression molding in a Carver press (Carver, Inc., Menomonee Falls, WI). A small amount of material, between two pieces of aluminum foil, was inserted for 2 min at 210°C without pressure to allow complete melting. After this, a pressure of 46 MPa was applied. After 2 min, with the pressure kept at 46 MPa, the samples were cooled to room temperature with a water-cooling system connected to the plates of the press. Then, the pressure was released, and the sheet was removed from the press.

Slabs 400 μm thick for mechanical tensile testing, wide-angle X-ray scattering (WAXS) measurements, and scanning electron microscopy (SEM) were prepared with the procedure used for the films, but with dimensions of 10 cm $\times$ 10 cm. The applied pressure was 23 MPa.

SEM

The surface analyses were performed with a Philips XL 20 series SEM microscope (Eindhoven, The Netherlands). Before observation, each sample was immersed in liquid nitrogen for 5 min and then was

broken, and the cryogenically fractured surfaces were coated with an Au–Pd alloy with an SEM coating device (BAL-TEC Mod. 020, Asslar, Germany).

WAXS measurements

WAXS measurements were carried out on a Philips XPW 1730 powder diffractometer (CuNi-filtered radiation) equipped with a rotating sample-holder device. The specimens of the blends were cut from the compression-molded samples. WAXS of HR MBG273 was performed on the sample as received.

The crystallinity percentage was calculated with the following procedure. The baseline was drawn between two points, which were chosen so that all diffraction patterns has minima at these points; the amorphous peak was chosen by a line being drawn that connected the two extreme minimum points of the baseline and the minimums of the crystalline peaks. The ratio of the area under the crystalline peaks to the total area, multiplied by 100, was taken as the crystallinity percentage.

The crystallinity fraction percentage, with reference to iPP, is the ratio, multiplied by 100, of the area under the crystallinity peaks to the sum of the area under the crystallinity peaks and the area of the amorphous peaks multiplied by the iPP percentage in the blend.

Optical microscopy

The optical observations were carried out with a Zeiss Axioscop MC100 polarizing optical microscope (Oberkochen, Germany) equipped with a Linkham TH600 hot stage and a Linkham TMS91 disposal for temperature control and regulation (Surrey, UK). A thin slice of the mixed material was inserted between two microscope cover glasses, melted, and squeezed to obtain a thin film with homogeneous thickness. The film was put on the hot-stage microscope and heated at 20°C/min from room temperature to 200°C and kept there for 10 min to eliminate the thermal history. Then, the material was quenched abruptly in air to room temperature as quickly as possibly to reproduce the industrial thermal cycle. Photographs were taken of the quenched films to investigate the morphology at room temperature after fast cooling.

Calorimetric measurements

The calorimetric properties of the blends were measured with a differential scanning calorimeter (Mettler DSC-30 with a TC11 processor and integrated software, Greifensee, Switzerland). The sample (ca. 10 mg) underwent two dynamic runs and one isothermal run in the following order: (1) it was heated from −100 to 200°C at a rate of 20°C/min (first dynamic run); (2) then, it was maintained in the isotherm at this last temperature for 10 min to allow melting and to delete every trace of previous crystallinity (isothermal run); and (3) finally, it was cooled from 200 to 25°C at a rate of 20°C/min (second dynamic run). Before each set of tests, a baseline was recorded with the same thermal program of the sample and subtracted from the thermogram of the sample. The measured thermal parameters were T_g and the melting temperature (T_m) on the thermoanalytical curves of the first dynamic run and the onset-of-crystallization and end-of-crystallization temperatures and the crystallization temperature (T_c) on the curves of the second dynamic run. T_m and T_c were valued at the maxima of the corresponding thermogram peaks.

Dynamic mechanical testing

DMTA data were collected at 1 Hz and at a heating rate of 2°C/min from −50 to 150°C under nitrogen with an MK III dynamic mechanical thermal analyzer (Polymer Laboratories, Darmstadt, Germany) configured for automatic data acquisition. The experiments were performed in the tensile mode on samples 40 mm long and 5 mm large cut from compression-molded films. The tan δ values were taken at the maximum of the tan δ curve and were considered to be T_g.

Mechanical tensile testing

Dumbbell-shaped specimens (type IV according to ASTM D 638) were cut from a slab with a steel punch cutter. Stress–strain curves were obtained with an Instron 4505 machine (High Wycombe, UK) at room temperature and at a crosshead speed of 5 mm/min. The modulus, stress, and elongation at rupture were calculated from such curves on an average of 24 specimens.

Water vapor permeability testing

Circular specimens (area = 30 cm^2, diameter = 6.182 cm) were cut from the films with a steel punch cutter of suitable shape and were used for water vapor permeability testing according to ASTM E 96 for the water method. The instrumental apparatus consisted of a test dish (Ceast, Torino, Italy), a test chamber (stove), and a balance (Mettler AE240). The test dish was made of steel, was circular, and had a 30-cm^2 mouth. Distilled water was used in the test dish, and the film was sealed to the test dish in such a way that the dish mouth defined the area of the specimen exposed to the vapor pressure in the dish. The test chamber was a stove in which the temperature was kept at 38.0 ± 0.2°C and the relative humidity of the air circulating was 10 ± 1%. The velocity of the air circulating over the specimens was sufficient to main-

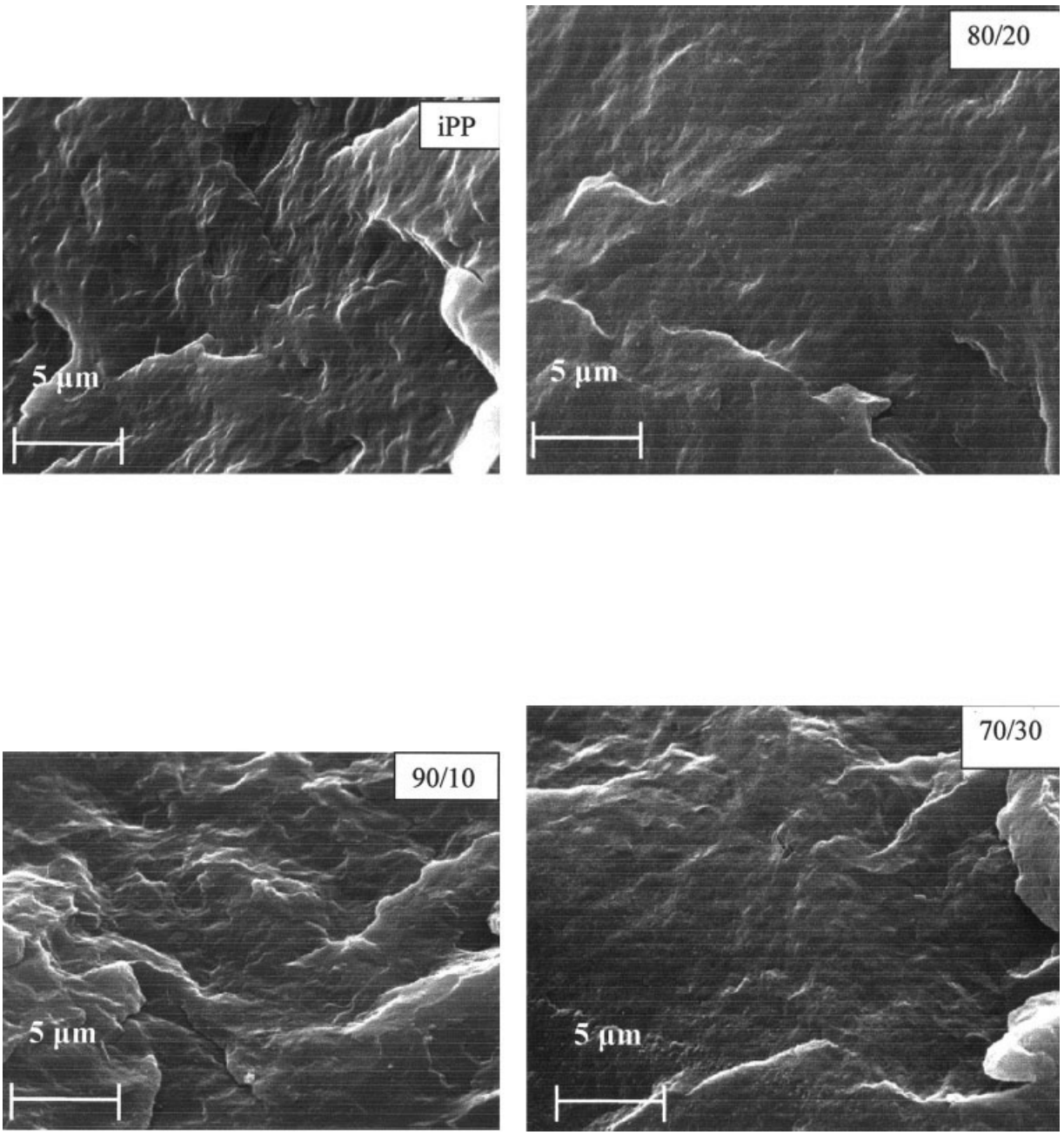

Figure 1 SEM micrographs of cryogenically fractured surfaces of compression-molded iPP/HR samples.

tain uniform conditions. The balance was sensitive to changes smaller than 1% of the weight change during the period when a steady state was considered to exist.

The test consisted of the gravimetric determination of the quantity of water vapor that passed through the surfaces (30 cm^2) of a film of suitable thickness (65–75 μm) in a fixed time (24 h) under precise conditions of relative air humidity (10% R.H.) and temperature (38°C).

The water vapor transmission rate (WVTR) is defined as the steady vapor flow in time through an area of a body, normal to specific parallel surfaces, under specific conditions of temperature and humidity at each surface.

The water vapor permeance is the time rate of water vapor transmission through the area of a flat material induced by a vapor pressure difference between two specific surfaces under specified temperature and humidity conditions.

The water vapor permeability is the time rate of water vapor transmission through an area of a flat material of a certain thickness induced by a vapor pressure difference between two specific surfaces under specified temperature and humidity conditions.

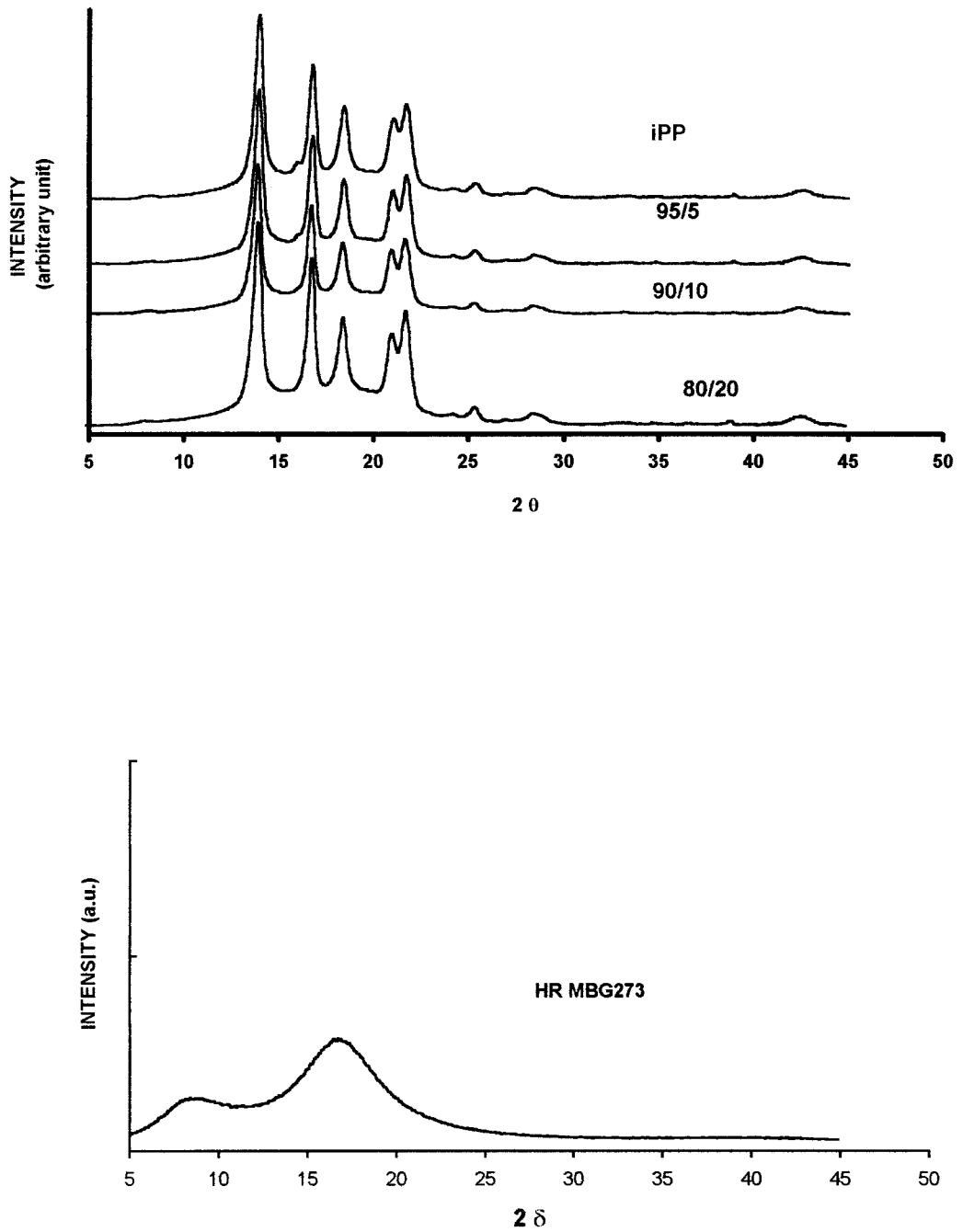

Figure 2 WAXS of HR, iPP, and iPP/HR blends.

RESULTS AND DISCUSSION

SEM

SEM micrographs of fractured surfaces of some iPP/HR MBG273 blends are given in Figure 1. No phase separation was observed for any of the samples investigated, and this indicated that iPP and HR formed a homogeneous phase in the amorphous phase, at least up to the HR content used in this work (30 wt %).

WAXS measurements

WAXS diffractograms are reported in Figure 2. The diffractogram of iPP indicates that the molecules crystallized in the monoclinic α form. The diffractogram of the HR shows a characteristic broad peak of the amorphous materials. The diffractograms of the blends show that the presence of HR did not induce any structural modification to the iPP α-monoclinic form for the blends investigated. Table I reports the crystallinity values of the blends and the values normalized

TABLE I
Crystallization Index from WAXS Diffractograms of Blends [X_c(blend)] and Values Normalized to iPP in the Blend [X_c(iPP)]

iPP/HR (wt %)	X_c(blend) (±4 %)	X_c (iPP) (±4 %)
100/0	54	54
97.5/2.5	54	54
95/5	52	54
90/10	49	52
85/15	46	53
80/20	44	54
70/30	41	54

to the iPP content in the blends (see the Experimental section for the calculation procedure). The crystallinity values normalized to the iPP content in the blends (third column) were constant with the composition (ca. 52–54%), indicating that the fraction of iPP found crystallized in any blend was the same. This behavior, that is, no influence of the resin on the polyolefin crystalline fraction, was also found for other systems, such as blends of iPP and natural terpene resins (PαP and PL),[1] iPP/HOCP blends,[15] high-density polyethylene/HOCP blends,[10] PB1/HOCP blends,[16] and P4MP1/HOCP blends.[17] In general, the presence of a resin in a blend, in the melt state, induces a decrease in the melt viscosity and influences the density of nucleation and the crystallization kinetics, but it does not have any influence on the number of crystallizable molecules. During the crystallization process, all the crystallizable material crystallizes; the presence of the resin has no influence.

Optical microscopy

Figure 3(A,B) shows optical micrographs of pure iPP and a 90/10 iPP/HR blend, respectively, abruptly quenched in air. Pure iPP crystallized according to a spherulitic morphology, with the spherulites dimensions varying from 30 to 100 μm. For the 90/10 iPP/HR blend [Fig. 3(B)], the iPP nucleation density decreased with respect to pure iPP. This effect was attributed to the diluent effect of HR for iPP molecules.

Calorimetric measurements

Figure 4 reports DSC thermograms registered during the cooling from the melt, at 20°C/min, of iPP and its blends with HR. The crystallization of plain iPP began at 115 ± 2°C and was completed at 81 ± 2°C, with a peak maximum at 102 ± 1°C. The presence of HR MBG273 delayed the iPP global crystallization process. This effect was larger for blends with higher HR contents. The thermograms of the compression-molded samples, registered at 20°C/min, are shown in Figure 5. The thermogram of iPP presents one endothermic peak due to the melting of monoclinic crystals, with a T_m, measured at peak maximum, of about 174 ± 1°C. The thermograms of the blends present T_m's lower than that of pure iPP. The analysis of the data indicates that T_m decreased significantly as the HR content in the blends increased. This decrease was attributed to a diluent effect of the HR component on the iPP crystals. The results of the DSC analysis are shown in Table II, which lists T_m, T_g, the enthalpy of melting of the blend [ΔH_m(blend)], and the value normalized to iPP contained in the blend [ΔH_m(iPP)]. The ΔH_m(iPP) results were constant, indicating that, in any blend, the crystallized fraction of iPP was the same, in agreement with the same trend found with WAXS analysis (see Table I, third column).

To investigate the influence of HR on the glass transition of iPP, we derived the thermograms from −40 to 100°C (see Fig. 6). The first derivative of the iPP curve indicated two transitions: the first at about 9

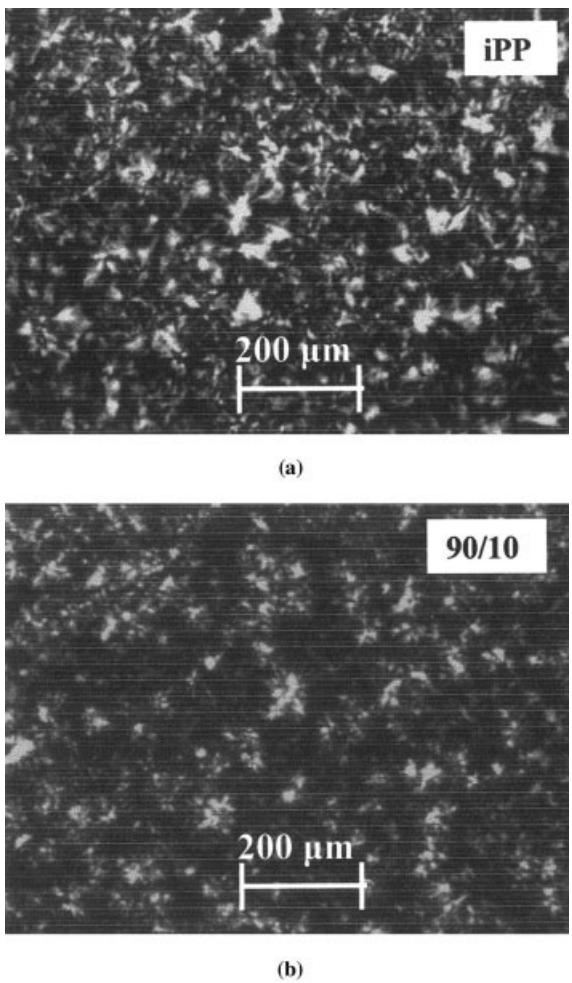

Figure 3 Optical micrographs of (A) 100/0 and (B) 90/10 iPP/HR films quenched abruptly in air.

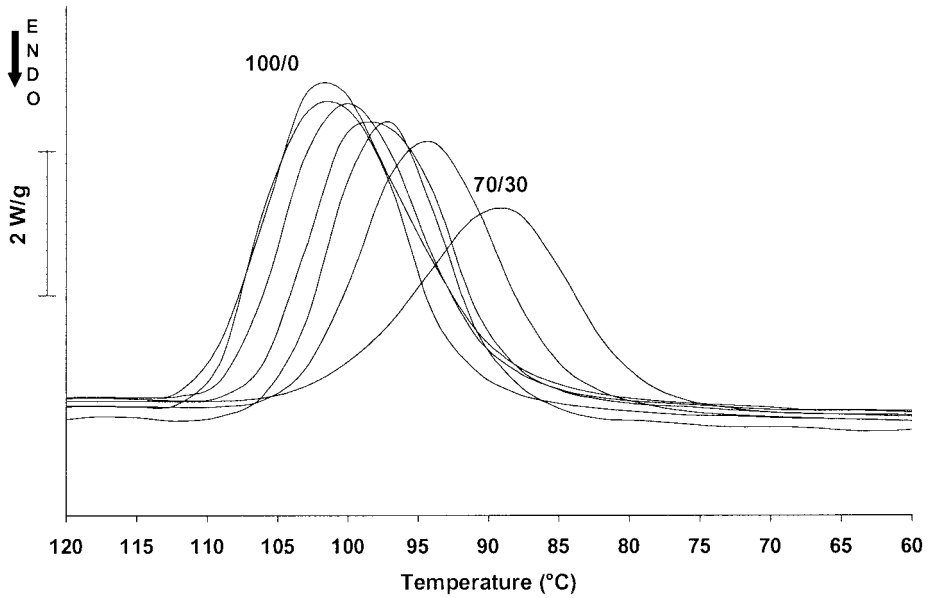

Figure 4 Thermoanalytical curves registered during the cooling from the melt of iPP/HR blends.

± 2°C and the second at about 48 ± 2°C. The appearance of two glass transitions in semicrystalline polymers is well known.[18–20] The transition at the lower temperature is generally attributed to the main T_g of iPP. The origin of the second transition at a higher temperature has been studied in the past with great attention.[18–20] To date, we agree with Boyer that this transition is to be attributed to an amorphous phase, that is, to the relaxation of molecules or a section of molecules interconnected to the crystalline phase as short cilia, loose loops, and tie molecules and not to the transition of molecules in the crystalline regions (generally indicated in the literature as T_c or $T\alpha_c$), which is generally located at a much higher temperature (see Fig. 5 in ref. 16). For iPP, there are several arguments in favor of the attribution of the transition at about 50°C to an amorphous transition [defined as T_g(U), i.e., the upper glass-transition temperature] instead of a crystalline transition. Boyer, in fact, analyzing in ref. 16 the work of other authors, reported the following: (1) about the work of Beck et al.,[21] he wrote, "Samples with 5 to 10% crystallinity apparently will

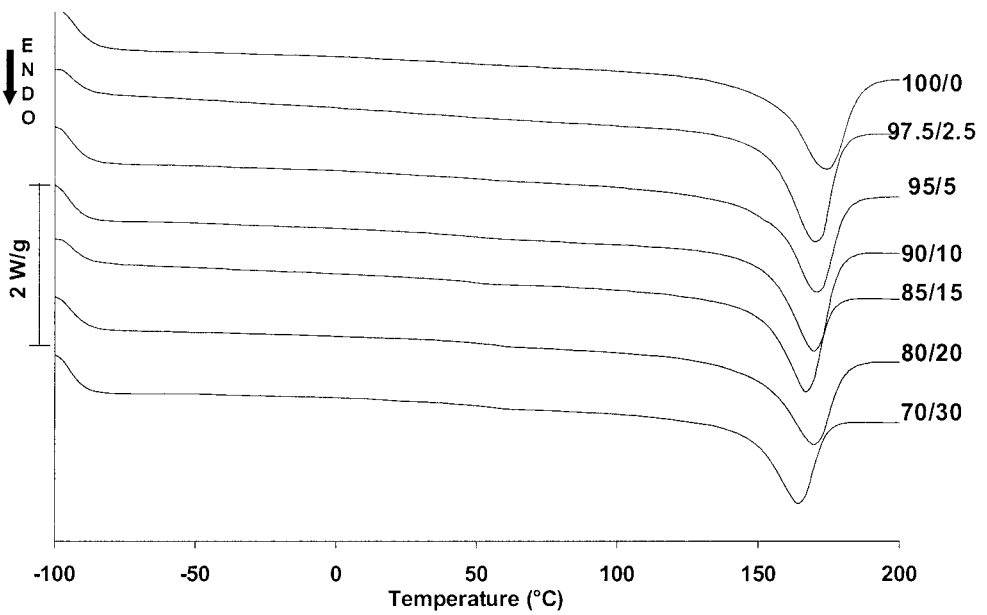

Figure 5 Thermoanalytical curves of iPP/HR blends.

TABLE II
Thermal Properties of iPP/HR Blends

iPP/HR (wt %)	T_m of iPP (±1 °C)	T_g(L) (±2 °C)	ΔH_m(blend) (±2 J/g)	ΔH_m(iPP) (± 2 J/g)
100/0	174	9	75	75
97.5/2.5	171	14	76	78
95/5	171	20	72	76
90/10	170	25	67	74
85/15	167	>30	63	74
80/20	168	>30	60	75
70/30	164	>30	53	75

not show a T_g(U) but do exhibit a T_c," and (2) about the work of Takayanagy,[22] he wrote, "Solution-grown single crystals of polypropylene show a strong T_c but only a very weak T_g(L). A highly quenched polypropylene exhibits only a strong T_g(L). If this quenched material is treated with fuming nitric acid to remove all amorphous material including loose loops and cilia, T_g(L) disappears and T_c is seen. Mild quenching brings out a double peak, T_g(L) and T_g(U)".

Therefore, in this article, the transitions at 9 ± 2°C are labeled T_g(L) (i.e., the lower glass-transition temperature), and the transition at 48 ± 2°C is labeled T_g(U).

Passing to the analysis of the first derivatives of the blend curves, we observed that the addition of HR MBG273 undoubtedly influenced T_g(L), which shifted gradually to a higher temperature until it merged with the peak of T_g(U). No transition at about 82 ± 2°C attributable to plain HR was observed. The absence of a transition attributable to plain HR, the continuous increase in T_g(L) with the MBG273 content, and the presence of homogeneous surfaces observed by SEM analysis for the blends indicated complete miscibility of MBG273 with the iPP amorphous phase.

To further verify the results obtained for the blends, we performed the following experiment: 9.5 mg of iPP and 4.1 mg of the MBG273 resin were put next to each other in the same sample DSC pan. The quantities used were similar to those of a virtual 70/30 blend. The following experiment was performed. The two components were heated to 210°C and kept at this temperature for 10 min to give them a thermal history like that of the 70/30 blend; then, the materials were cooled to −80°C at 50°C/min, and finally they were heated again up to 200°C at 20°C/min. The thermoanalytical curve of this virtual 70/30 blend (i.e., iPP and MBG273 in the same DSC pan) is reported in Figure 7, and the relative first derivative curve is given in Figure 8 together with the first derivative curves of the thermogram curves of MBG273, iPP, and the 70/30 blend, for easier comparison. The first derivative curve shows the presence of three peaks: the first is centered at about 0°C and is attributed to T_g(L) of iPP, the second peak is centered at about 50°C and is due

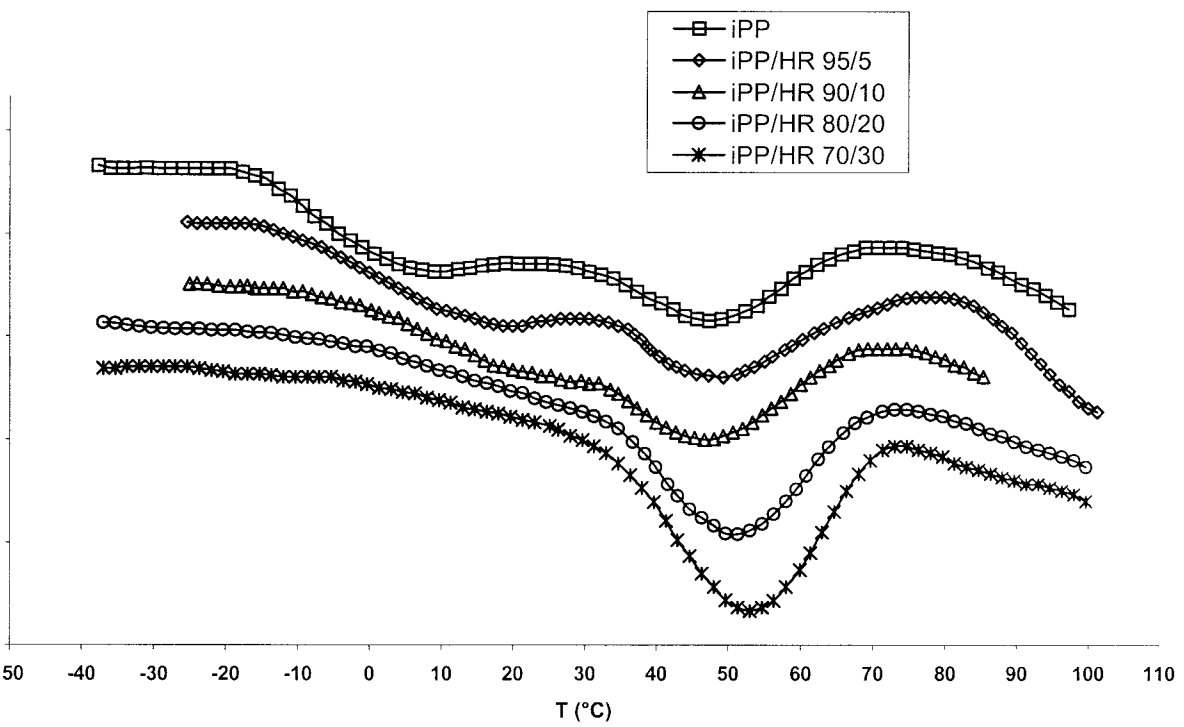

Figure 6 First derivative of DSC thermograms of iPP/HR blends.

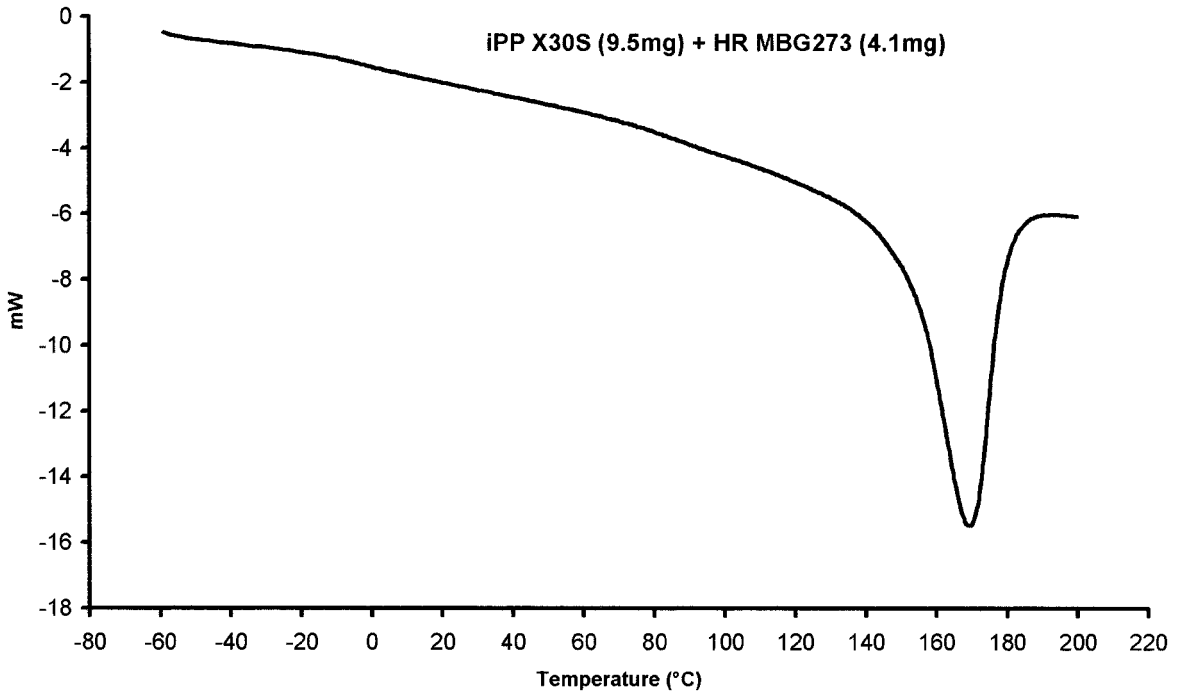

Figure 7 Thermoanalytical curve of iPP and HR MBG273 contained in the same sample DSC pan.

to T_g(U) of iPP, and the third one is due to T_g of MBG273. From a comparison of the curve of the 70/30 blend (showing only one peak) and the curve of iPP+ MBG273 (with three peaks), it is plausible to conclude that only one homogeneous phase is formed when iPP and MBG273 are melt-mixed.

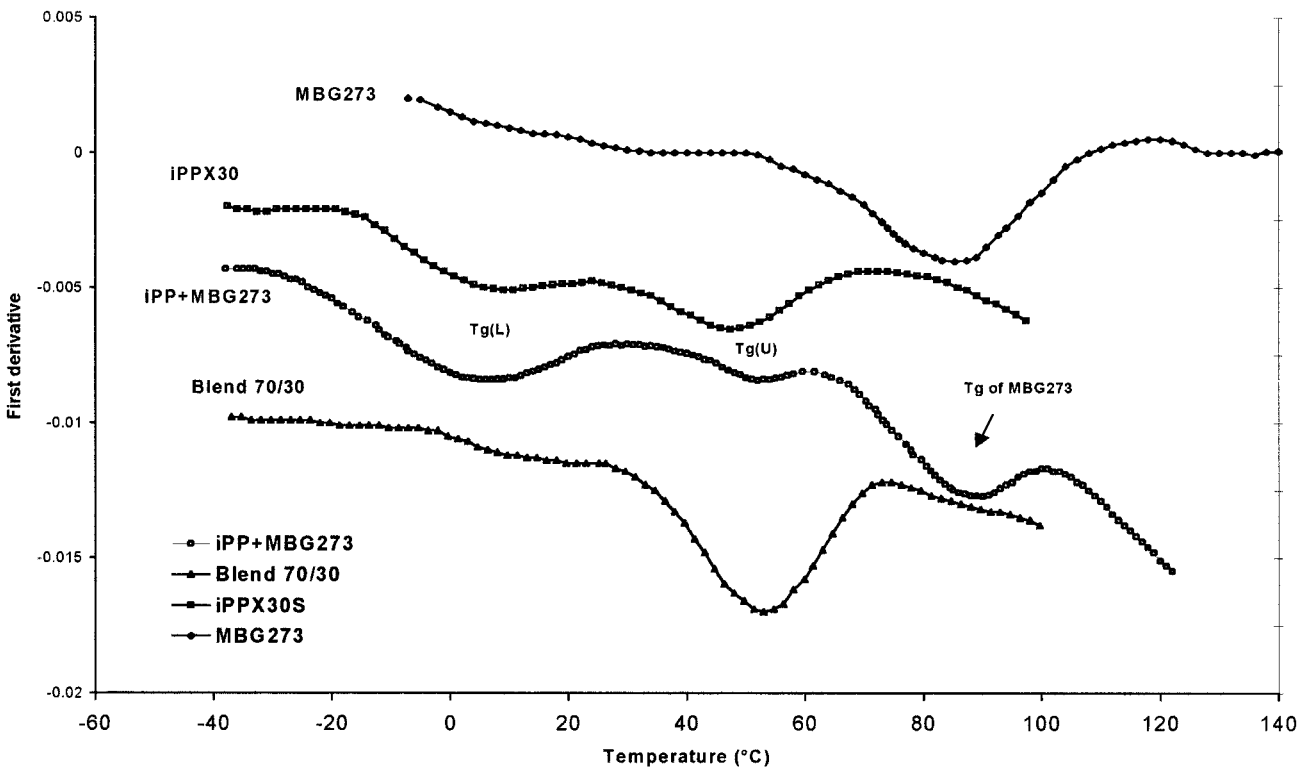

Figure 8 First derivative curves of thermograms of iPP X30S, HR MBG273, a 70/30 blend, and iPP/MBG273.

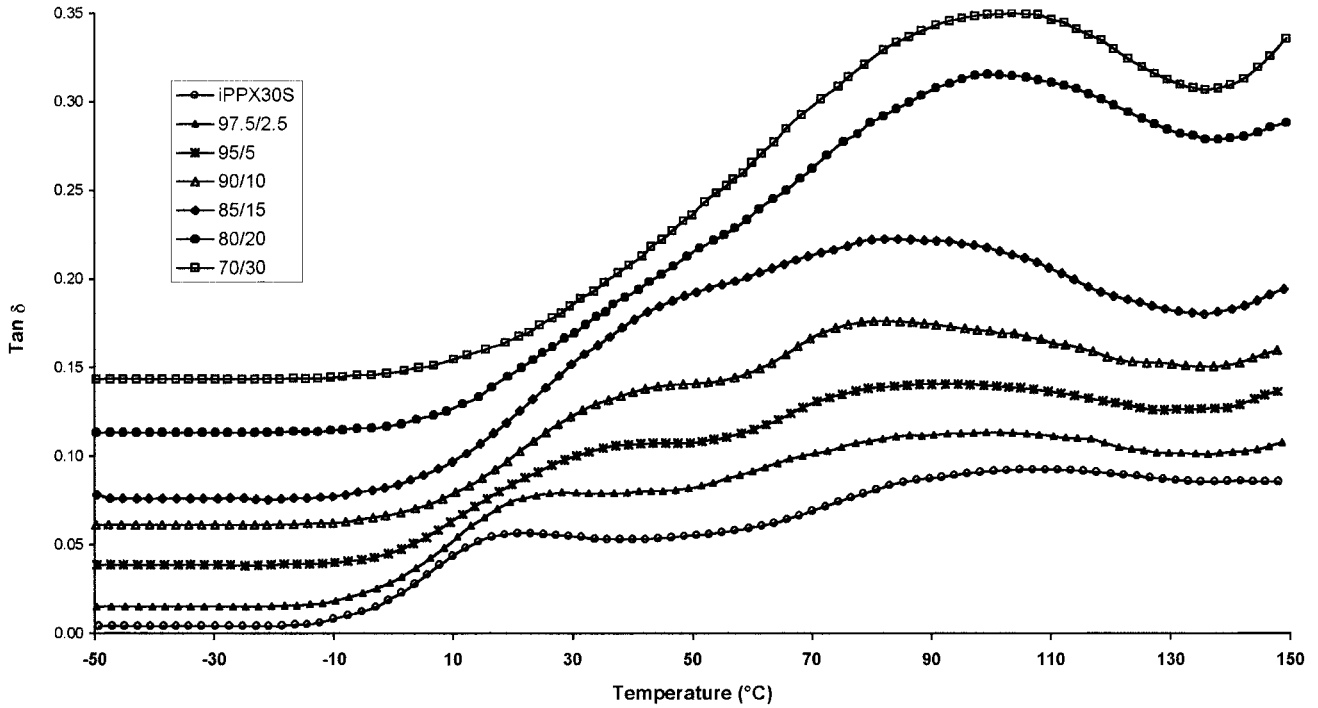

Figure 9 Tan δ of iPP/HR blends.

DMTA

Figure 9 reports tan δ as a function of temperature for the various samples. Tan δ of iPP presents two peaks: the first is attributed to T_g(L) at about 15 ± 2°C and the second, very broad, from 50 to 130°C, is attributed to T_g(U). For the blends with up to 15% HR, the tan δ peak of T_g(L) shifted gradually to a higher temperature as the MBG273 content increased, whereas the tan δ peak of T_g(U) seemed to be unaffected by the presence of HR in the blends, as found from the first derivatives of DSC thermoanalytical curves. For the 80/20 and 70/30 blends, the peak at the lower temperature could not be observed anymore, and only one large peak, centered around 100°C, was present. These results further indicate that MBG273 and amorphous iPP formed one homogeneous amorphous phase in the blends.

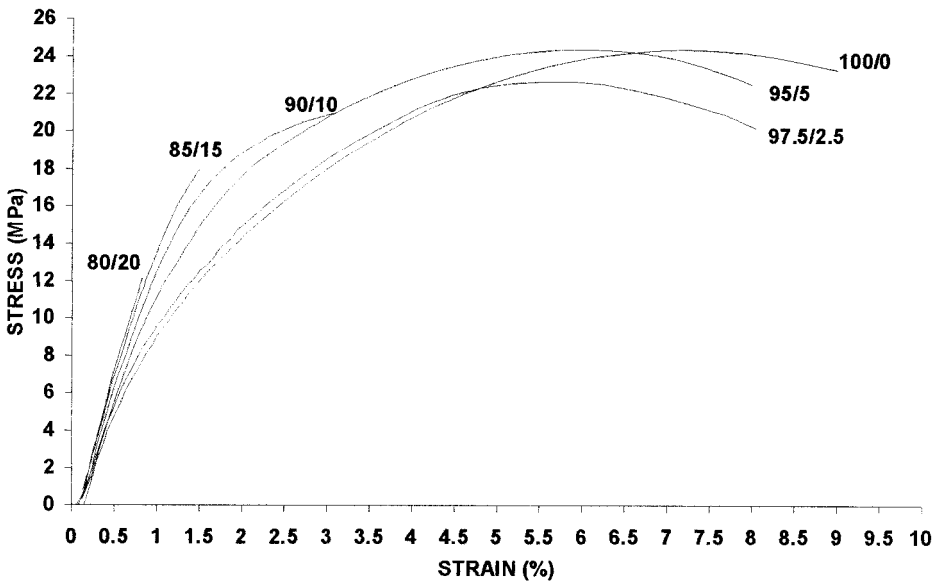

Figure 10 Stress–strain curves of iPP/HR blends.

TABLE III
Mechanical Properties of iPP/HR Blends

iPP/HR (wt %)	E (MPa)	σ_b (MPa)[a]	ε_b (%)[b]
100/0	970 ± 80	23 ± 2	9 ± 1
97.5/2.5	1060 ± 50	20 ± 2	8 ± 1
95/5	1380 ± 30	22 ± 2	8 ± 1
90/10	1490 ± 70	20 ± 2	3 ± 1
85/15	1870 ± 60	19 ± 2	1.4 ± 0.1
80/20	1890 ± 60	13 ± 3	0.9 ± 0.2
70/30	2365 ± 90	13 ± 2	0.7 ± 0.1

[a] σ_b = stress at break point.
[b] ε_b = elongation at break point.

Mechanical tensile testing

Nominal stress–strain curves of iPP/HR samples, tested at room temperature at a crosshead speed of 5 mm/min, are presented in Figure 10. All the tensile parameters are reported in Table III. The behaviors of the blends depended on the MBG273 content. Young's modulus (E) increased with the resin content. The ultimate properties (σ_b and ε_b) were strongly influenced by the presence of MBG273. Blends with MBG273 contents lower than 10% showed tensile behavior similar to that of plain iPP. Blends with MBG273 contents higher than 10% showed brittle behavior characterized by a low value of ε_b. The tensile behaviors could be interpreted as follows: at room temperature, the addition of MBG273 to iPP changed the physical state of amorphous iPP from a rubbery phase to a glassy phase, making the system harder. The values of E depended on two opposing factors: the overall crystallinity and the physical state of the amorphous phase. The decrease in the overall crystallinity with the HR content, observed by WAXS results, reduced E. The hardening of the amorphous phase, due to HR molecules that increased T_g of the system, increased E. The second effect was predominant over the first one, and the overall balance was an increase in E.

Water vapor permeability test

The water vapor permeability test was conducted only on plain iPP and films containing up to 10 wt % HR, that is, films potentially interesting for packaging applications in industry. Films with higher resin contents were very brittle (see the section on the tensile properties).

The results of the water vapor permeability testing of pure iPP and 95/5 and 90/10 blends are shown in Table IV.

These results indicate that the addition of HR to iPP lowered the water vapor permeability. The data show that a content of 5% HR in a blend reduced the water vapor permeability by 28%, whereas 10% HR lowered the water vapor permeability by 42%. The permeability values of a semicrystalline polymer such as iPP depend on two factors: the crystallinity fraction and the physical state of the amorphous phase. The crystalline phase is considered impermeable to gas, and so the higher the crystallinity fraction is, the lower the permeability value is. The rubbery amorphous phase is more permeable to gas than the glassy amorphous phase, and so the harder the amorphous phase is, the lower the permeability value is. In the iPP/HR blends, the presence of HR reduced the overall crystallinity of the material and, at the same time, made the amorphous phase of iPP more rigid. The overall effect was that the second factor was predominant over the first, as found also for E, and so the water vapor permeability decreased.

CONCLUSIONS

iPP/HR blends in the solid state formed a two-phase system composed of a crystalline phase of iPP in an α-monoclinic form and an amorphous phase formed of amorphous iPP and HR, the T_g of which increased with the resin content. The hypothesis of the formation of only one amorphous phase consisting of iPP and HR closely mixed seemed quite reliable according to the SEM, DSC, and DMTA results. The analysis of blend thermograms, registered during the cooling from the melt, indicated that HR caused a decrease in the overall crystallization kinetic. Optical microscopy observations of blends quenched in air from the melt showed that iPP crystallized according to a spherulite morphology and that the presence of HR in the iPP matrix reduced the iPP nucleation density, causing an increase in the iPP spherulite dimensions. The analysis of the tensile properties showed that the presence of HR in amorphous iPP increased E. The parameters at break of blends with up to 10 wt % HR were similar to those of pure iPP. Blends

TABLE IV
Water Vapor Properties of iPP/HR Blends

iPP/HR (wt %)	WVTR [±0.8 g/(24 h m^2)]	Permeance [±1.6 ng/(Pa s m^2)]	Permeability [±0.15 ng/(Pa s m)]
100/0	31.5	61.0	4.27
95/5	22.8	44.3	3.10
90/10	18.4	35.7	2.50

with higher HR contents were very brittle, with low elongation at break and strength at break. The analysis of the water vapor permeability, according to the increase in T_g(L), showed a remarkable decrease in the water vapor permeability as the HR was added to iPP.

The authors thank G. Loeber (Eastman Co.) for the MBG273 hydrocarbon resin and for his helpful discussion about the analysis of the data and film applications.

References

1. Cimmino, S.; D'Alma, E.; Di Lorenzo, M. L.; Di Pace, E.; Silvestre, C. J Polym Sci Part B: Polym Phys 1999, 37, 867.
2. Silvestre, C.; Cimmino, S.; Di Lorenzo, M. L. J Appl Polym Sci 1999, 71, 1677.
3. Di Lorenzo, M. L.; Cimmino, S.; Silvestre, C. J Appl Polym Sci 2001, 82, 358.
4. Cimmino, S.; Greco, R.; Iavarone, M.; Silvestre, C. In preparation.
5. Silvestre, C.; Cimmino, S.; Di Pace, E.; Di Lorenzo, M. L.; Monaco, M. J Macromol Sci Phys 1996, 35, 457.
6. Cimmino, S.; Guarrata, P.; Martuscelli, E.; Silvestre, C.; Buzio, P. P. Polymer 1991, 32, 3299.
7. Cimmino, S.; Di Pace, E.; Karasz, F. E.; Martuscelli, E.; Silvestre, C. Polymer 1993, 34, 972,.
8. Cimmino, S.; Martuscelli, E.; Silvestre, C. Makromol Chem Macromol Symp 1994, 78, 115.
9. Cimmino, S.; Di Pace, E.; Martuscelli, E.; Mendes, L. C.; Silvestre, C. J Polym Sci 1994, 32, 2025.
10. Cimmino, S.; Di Pace, E.; Martuscelli, E.; Silvestre, C.; Mendes, L. C.; Bonfanti, G. J Polym Sci Part B: Polym Phys 1995, 33, 1723.
11. Caponetti, E.; Chillura Martino, D.; Cimmino, S.; Floriano, M. A.; Martuscelli, E.; Silvestre, C.; Triolo, R. J Mol Struct 1996, 383, 75.
12. Buzio, P.; Marcandalli, B.; Martuscelli, E.; Seves, A. Ital. Pat. 22196A (1990).
13. Silvestre, C.; Cimmino, S.; D'Alma, E.; Di Lorenzo, M. L.; Di Pace, E. Polymer 1999, 40, 5119.
14. Findlay, J. In Encyclopedia of Polymer Science and Engineering; Mark, H. F.; Bikales, N. M.; Overberger, C. G.; Menges, G.; Kroschwitz, J. I., Eds.; Wiley: New York, 1987; Vol. 9, p 853.
15. Cecere, A.; Greco, R.; Taglialatela, A. Polymer 1992, 33, 1411.
16. Cimmino, S.; Di Lorenzo, M. L.; Di Pace, E.; Silvestre, C. J Appl Polym Sci 1998, 67, 1369.
17. Cimmino, S.; Monaco, M.; Silvestre, C. J Polym Sci Part B: Polym Phys 1997, 35, 1269.
18. Boyer, R. F. J Polym Sci 1975, 50, 189.
19. Boyer, R. F. J Macromol Sci Phys 1973, 8, 503.
20. Geil, P. H. In Order in the Amorphous State of Polymers; Keinath, S. E.; Miller, R. L.; Rieke, J. K., Eds.; Plenum: New York, 1987; p 83.
21. Beck, L.; Hiltz, A. A.; Knox, J. R. Soc Plast Eng Trans 1963, 3, 279.
22. Takayanagy, M. Pure Appl Chem 1967, 15, 555.